Virology 425 (2012) 31–39

Contents lists available at SciVerse ScienceDirect

Virology

journal homepage: www.elsevier.com/locate/yviro

Matrigel-embedded 3D culture of Huh-7 cells as a hepatocyte-like polarized system to study hepatitis C virus cycle

Francisca Molina-Jimenez [a,b,1], Ignacio Benedicto [a,b,1], Viet Loan Dao Thi [c,d,e], Virginia Gondar [a], Dimitri Lavillette [c,d,e], Jose J. Marin [b,f], Oscar Briz [b,g], Ricardo Moreno-Otero [b,h], Rafael Aldabe [b,i], Thomas F. Baumert [j], François-Loïc Cosset [c,d,e], Manuel Lopez-Cabrera [a,b,k], Pedro L. Majano [a,b,*]

[a] Molecular Biology Unit, Hospital Universitario de la Princesa, Instituto de Investigación Sanitaria Princesa (IP), Madrid 28006, Spain
[b] CIBERehd, Instituto de Salud Carlos III, Madrid 28029, Spain
[c] Université de Lyon, UCB-Lyon1, IFR128, Lyon F-69007, France
[d] INSERM, U758, Lyon F-69007, France
[e] Ecole Normale Supérieure de Lyon, Lyon F-69007, France
[f] Laboratory of Experimental Hepatology and Drug Targeting, Universidad de Salamanca, Salamanca 37007, Spain
[g] Research Unit, Hospital Universitario de Salamanca, Salamanca 37007, Spain
[h] Liver Unit, Hospital Universitario de la Princesa, Instituto de Investigación Sanitaria Princesa (IP), Madrid 28006, Spain
[i] Division of Gene Therapy and Hepatology, Centro de Investigación en Medicina Aplicada, CIMA, Pamplona 31008, Spain
[j] Inserm U748, Université de Strasbourg, F-67000 Strasbourg, France
[k] Centro de Biología Molecular Severo Ochoa, CSIC-UAM, Madrid 28049, Spain

ARTICLE INFO

Article history:
Received 20 October 2011
Returned to author for revision
11 November 2011
Accepted 31 December 2011
Available online 24 January 2012

Keywords:
HCV infection
Three dimensional cultures
Tight junctions
Cellular polarization
Bile canaliculi

ABSTRACT

Hepatocytes are highly polarized cells where intercellular junctions, including tight junctions (TJs), determine the polarity. Recently, the TJ-associated proteins claudin-1 and occludin have been implicated in hepatitis C virus (HCV) entry and spread. Nevertheless, cell line-based experimental systems that exhibit hepatocyte-like polarity and permit robust infection and virion production are not currently available. Thus, we sought to determine whether cell line-based, Matrigel-embedded cultures could be used to study hepatitis C virus (HCV) infection and virion production in a context of hepatocyte-like polarized cells. In contrast to standard bidimensional cultures, Matrigel-cultured Huh-7 cells adopted hepatocyte polarization features forming a continuous network of functional proto-bile canaliculi structures. These 3D cultures supported HCV infection by JFH-1 virus and produced infective viral particles which shifted towards lower densities with higher associated specific infectivity. In conclusion, our findings describe a novel use of Matrigel to study the entire HCV cycle in a more relevant context.

Introduction

In a high percentage of patients, acute hepatitis C virus (HCV) infections become chronic and ultimately progress to fibrosis, cirrhosis and hepatocellular carcinoma (Poynard et al., 2003). Therapy consisting of a combination of pegylated interferon-alpha plus ribavirin is limited by a response rate of less than 50% in patients infected with genotype 1 (Feld and Hoofnagle, 2005), which can be considerably improved by the inclusion of the HCV protease inhibitors boceprevir or telaprevir as part of a triple therapy (Hofmann and Zeuzem, 2011). HCV, belonging to the *Flaviviridae* family, is a small enveloped RNA virus mainly transmitted by blood and other body fluids (Lindenbach and Rice, 2005). In plasma, HCV RNA-containing particles can be found associated with lipoproteins, which have been suggested to play a role in early steps of HCV infection (Andre et al., 2005). Multiple evidence exists for the involvement of host cell factors in HCV entry, including glycosaminoglycans, the low-density lipoprotein receptor, scavenger receptor class B type I (SR-BI), the

Abbreviations: HCV, hepatitis C virus; SR-BI, scavenger receptor class B type I; TJ(s), tight junction(s); BC, bile canaliculi; ZO-1, zonula occludens protein-1; HCVcc, cell culture derived HCV; CMFDA, 5-chloromethylfluorescein di-acetate; CGamF, cholylglycylamido fluorescein; IFN-α, interferon-alpha; shRNA, short hairpin RNA; MRP2, multidrug resistance-associated protein 2; PHH, primary human hepatocytes; VLDLs, very low density lipoproteins.

* Corresponding author at: Unidad de Biología Molecular, Hospital Universitario de la Princesa, C/Diego de León 62, 28006 Madrid, Spain. Fax: +34 91 3093911.
E-mail addresses: fmolina.hlpr@salud.madrid.org (F. Molina-Jimenez), ibenedicto.hlpr@salud.madrid.org (I. Benedicto), viet.loan.dao.thi@ens-lyon.fr (V.L. Dao Thi), virginiagondar@gmail.com (V. Gondar), Dimitri.Lavillette@ens-lyon.fr (D. Lavillette), jjgmarin@usal.es (J.J. Marin), obriz@usal.es (O. Briz), rmoreno.hlpr@salud.madrid.org (R. Moreno-Otero), raldabe@unav.es (R. Aldabe), Thomas.Baumert@unistra.fr (T.F. Baumert), flcosset@ens-lyon.fr (F.-L. Cosset), mlopez.hlpr@salud.madrid.org (M. Lopez-Cabrera), pmajano.hlpr@salud.madrid.org (P.L. Majano).
[1] These authors contributed equally to this work.

0042-6822/$ – see front matter.
doi:10.1016/j.virol.2011.12.021

tetraspanin CD81 and the tight junction (TJ) proteins claudin-1 and occludin (Zeisel et al., 2011).

The correct functioning of the liver is ensured by the setting and maintenance of the highly polarized phenotype of hepatocytes. In contact with the external environment, the apical poles of front-facing and adjacent hepatocytes form a continuous network of bile canaliculi (BC) where bile is secreted (Easter et al., 1983). TJs maintain cell polarity separating apical from basolateral membrane domains and form a paracellular barrier that allows the selective passage of certain solutes (Aijaz et al., 2006). In hepatocytes, TJs seal the bile canaliculi and form the intercellular barrier between bile and blood (Easter et al., 1983). Human hepatocyte-derived cell lines susceptible to HCV infection such as Huh-7 barely form BC structures, but TJ-associated proteins such as zonula occludens protein-1 (ZO-1), occludin and claudin-1 form belts at the cell apex as in 'simple' polarized cells (Benedicto et al., 2008; Benedicto et al., 2009). Thus, although TJ-associated proteins in these systems exert, at least to some extent, their typical functions (i. e., separate apical from basolateral domains and constitute a paracellular barrier), cellular models displaying hepatocyte-like polarity are needed to study HCV life cycle in a more physiologically relevant context (Gondeau et al., 2009; Perrault and Pecheur, 2009).

To date, it is not clearly established how hepatocyte polarity influences HCV cycle (Perrault and Pecheur, 2009). Several attempts have been carried out to reproduce the in vivo phenotype of hepatocytes in 3D-cultured cell lines and propagate HCV by using different kinds of bioreactors (Sainz et al., 2009). Despite cells were susceptible to infection and produced new infectious virions, no evidence was found to support the polarized localization of basolateral and apical markers or the existence of functional BC-like structures. Furthermore, HepG2 cells ectopically expressing CD81 have been used as a model of polarized culture to study HCV infection (Mee et al., 2009), but their restricted efficiency to support infection (more than 700-fold reduction compared to Huh-7.5 cells) (Lindenbach et al., 2005; Mee et al., 2009) limits their use as a system to study HCV assembly and egress. Recently, it has been shown that ectopic expression of the microRNA miR-122 in HepG2-CD81 cells increases their HCV RNA replication efficiency, although infectious viral release was still 10- to 50-fold reduced

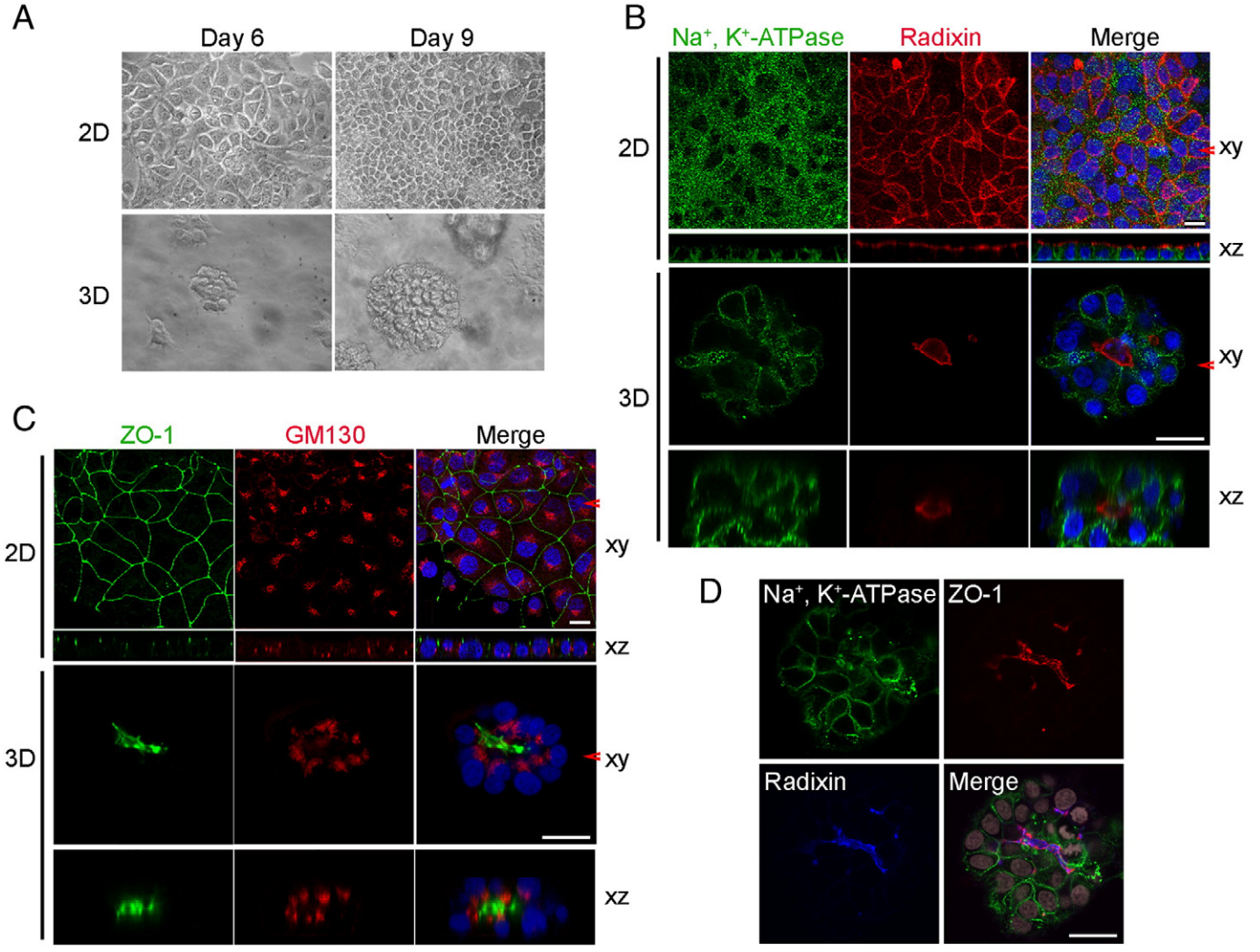

Fig. 1. Characterization of Matrigel-embedded 3D aggregates of the human hepatocyte-derived cell line Huh-7. (A) Phase contrast image (20× magnification) of 2D and 3D Huh-7 cultures 6 and 9 days after seeding. (B and C) Cells were grown in 2D and 3D conditions for 6 days and processed for double-label immunofluorescence and confocal analysis. Na^+, K^+-ATPase (basolateral marker) and ZO-1, green; radixin (apical marker) and GM130 (a Golgi matrix protein), red; nuclei were stained with DAPI (blue). 2D images show the merged projection of confocal stacks (XY, top) and XZ sections (bottom). 3D images show a single XY section from the confocal stacks (top) and XZ sections (bottom). Arrows indicate the plane from which the Z sections were taken. Z sections were compiled by taking 0.5 μm steps through each XY section. Photographs are representative of at least three separate experiments. Bar, 25 μm. (D) Cells were grown in 3D conditions and processed for immunofluorescence and confocal analysis as in (B) and (C). Images show a single XY section from the confocal stacks. Na^+, K^+-ATPase, green; ZO-1, red; radixin, blue; nuclei were stained with DAPI (gray). Bar, 25 μm.

compared to Huh-7.5 cells (Narbus et al., 2011). Herein, we describe that Matrigel-embedded cultures of the human hepatoma-derived cell line Huh-7 can be used as a robust, 3D hepatocyte-like polarized system to study the entire HCV cycle.

Results

Characterization of 3D cultures of human hepatocyte-derived cell lines

Matrigel is the trade name for a gelatinous protein mixture secreted by Engelbreth–Holm–Swarm mouse sarcoma cells that resembles the complex extracellular environment found in many tissues and is used to produce thick 3D gels for cell culture (Kleinman and Martin, 2005). It was observed that Matrigel-cultured Huh-7 cells assembled into 3D spheroids, whereas standard 2D-cultured cells formed the typical epithelial monolayer (Fig. 1A). In 2D cultures, Na^+, K^+-ATPase was distributed basolaterally and radixin mainly localized to the apical pole of cells, resembling a 'simple' epithelial phenotype (Fig. 1B, top). In 3D cultures, both markers were also mutually exclusive; however, spheroids presented a canalicular-like radixin staining localized at membranes surrounding the lumens within 3D aggregates (Fig. 1B, bottom and Fig. 1D). Furthermore, in 2D cultures ZO-1 was confined to cell-cell junctions as in cells with 'simple' epithelial polarization, and the Golgi apparatus did not show any specific orientation within cells (Fig. 1C, top). In contrast, and similarly to polarized hepatocytes, the Golgi apparatus of spheroid-forming cells was clearly positioned between the nuclei and the lumen, whose edges were positive for ZO-1 (Fig. 1C, bottom, Fig. 1D and Supplementary Fig. S1). Overall, these data suggested that 3D-cultures presented hepatocyte-like polarization and developed TJ-delimited canalicular structures.

Hepatocyte apical domain is designed for the secretion of bile into BC (Easter et al., 1983). Among other proteins, radixin is a critical requirement for the normal maintenance of the canalicular membrane and the localization and function of its transport proteins (Wang et al., 2006). As shown in Figs. 1B and 1D, radixin localized around the lumen of spheroids, suggesting that the apical membranes might behave as functional bile secretion domains. To further investigate the functionality of these BC-like structures, we next analyzed the expression levels and subcellular localization of the multidrug resistance protein 2 (MRP2), essential for the secretory function of differentiated hepatocytes. We analyzed MRP2 mRNA and protein levels and observed no evident differences between 2D and 3D cultures (Fig. 2A and data not shown). However, whereas in 2D cultures MRP2 was not concentrated at any particular localization, 3D spheroids presented a marked accumulation of MRP2 at the membranes delimiting the BC-like structure (Fig. 2B). Furthermore, to analyze the cell export ability of 2D and 3D cultures, they were loaded with the general cell stain 5-chloromethylfluorescein di-acetate (CMFDA) or the conjugated bile acid analog cholylglycylamido fluorescein (CGamF) (see Materials and Methods) and visualized by confocal microscopy. 2D-cultured cells were not able to secrete the compounds, as evidenced by a clear intracellular retention (Fig. 2C). In contrast, spheroid-forming cells efficiently exported the labeled molecules to the canalicular space where they accumulated (Fig. 2C). Interestingly, CMFDA transport was blocked in the presence of the MRP2 inhibitor Probenecid (Fig. 2C). These data strongly suggested that, in contrast to standard 2D cultures, 3D spheroids developed BC-like structures that presented vectorial trafficking of compounds. In summary, 3D-cultured Huh-7 cells displayed structural and functional polarity features similar to hepatocytes in vivo. In order to study whether

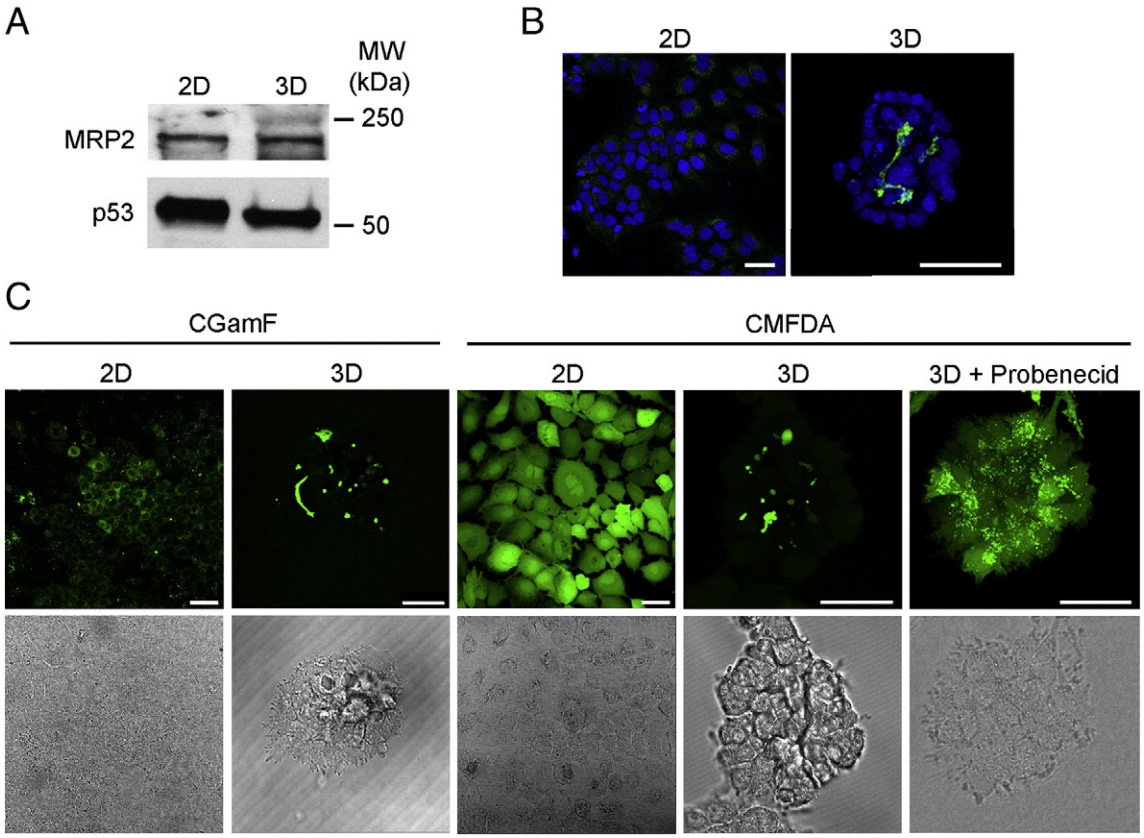

Fig. 2. BC-like structure and function in 2D and 3D-cultured Huh-7 cells. (A) MRP2 protein levels were analyzed by Western blot. p53 was used as loading control. Molecular weight markers (kDa) are indicated on the right. (B) MRP2 localization after 6 days of 2D and 3D culture was analyzed by confocal immunofluorescence analysis. Images show the merged projection of confocal stacks. MRP2, green; nuclei, blue. Bar, 50 μm. (C) Cells were 2D or 3D cultured for 6 days, treated with 5 μM CMFDA or CGamF and washed in the presence (5 mM) or absence of Probenecid. Confocal images show the accumulation of CMFDA and CGamF. Bar, 50 μm. Results shown are representative of at least three separate experiments.

the differentiation of Huh-7 cells was improved in 3D cultures, we analyzed the expression of hepatocyte-specific markers by real-time RT-PCR and no major changes were observed (Supplementary Fig. S2).

3D cultures are susceptible to HCV infection

Firstly, we compared the expression levels of the HCV (co)receptors SR-BI, CD81, occludin and claudin-1 between 2D and 3D cultures by Western blot analysis, and no substantial differences were found (Fig. 3A). We next analyzed whether the localization of the HCV (co)receptors in 3D cultures was altered when compared to 2D cultures. Similar to previous studies (Benedicto et al., 2008, 2009), staining of occludin and claudin-1 in 2D cultures appeared to localize at the apical poles of lateral cell membranes, the typical distribution of these proteins in cells with 'simple' epithelial polarization (Fig. 3B and Supplementary Fig. S3). However, in 3D cultures occludin and claudin-1 seemed to present a similar localization as ZO-1 (Fig. 1 C and Supplementary Fig. S3), being mainly detected surrounding the BC-like structures. These results are in agreement with the localization of claudin-1 in polarized HepG2 cells (Harris et al., 2010) and the distribution of occludin and claudin-1 in liver biopsies (Mee et al., 2009). Additionally, we could not show any evidence to support that 3D conditions promoted the redistribution of CD81 and SR-BI, which in both 2D and 3D cultures appeared distributed throughout the plasma membrane (Fig. 3B). These results fit well with data obtained from non-polarized and polarized HepG2-CD81 cells (Mee et al., 2009). In summary, our results indicated that embedding Huh-7 cells in Matrigel did not significantly affect the expression levels of the HCV (co)receptors analyzed but altered the spatial distribution of occludin and claudin-1, which were concentrated at hepatocytic-like TJ structures. Nevertheless, we cannot rule out a possible extrajunctional, diffuse localization of a pool of TJ-associated proteins, which has been already described in other polarized systems (Harris et al., 2010).

We next sought to determine whether 3D cultures were susceptible to HCV infection. We performed infection assays using HCVcc and 2D or 3D-cultured Huh-7 cells, and monitored viral RNA at different time points post-infection by real-time RT-PCR (Fig. 3C). We also included controls without cells in both 2D and 3D conditions (data not shown). HCV RNA was only detected when cells were present; in addition, viral RNA levels increased with time, demonstrating that the signal obtained was not due to the amplification of Matrigel-bound input

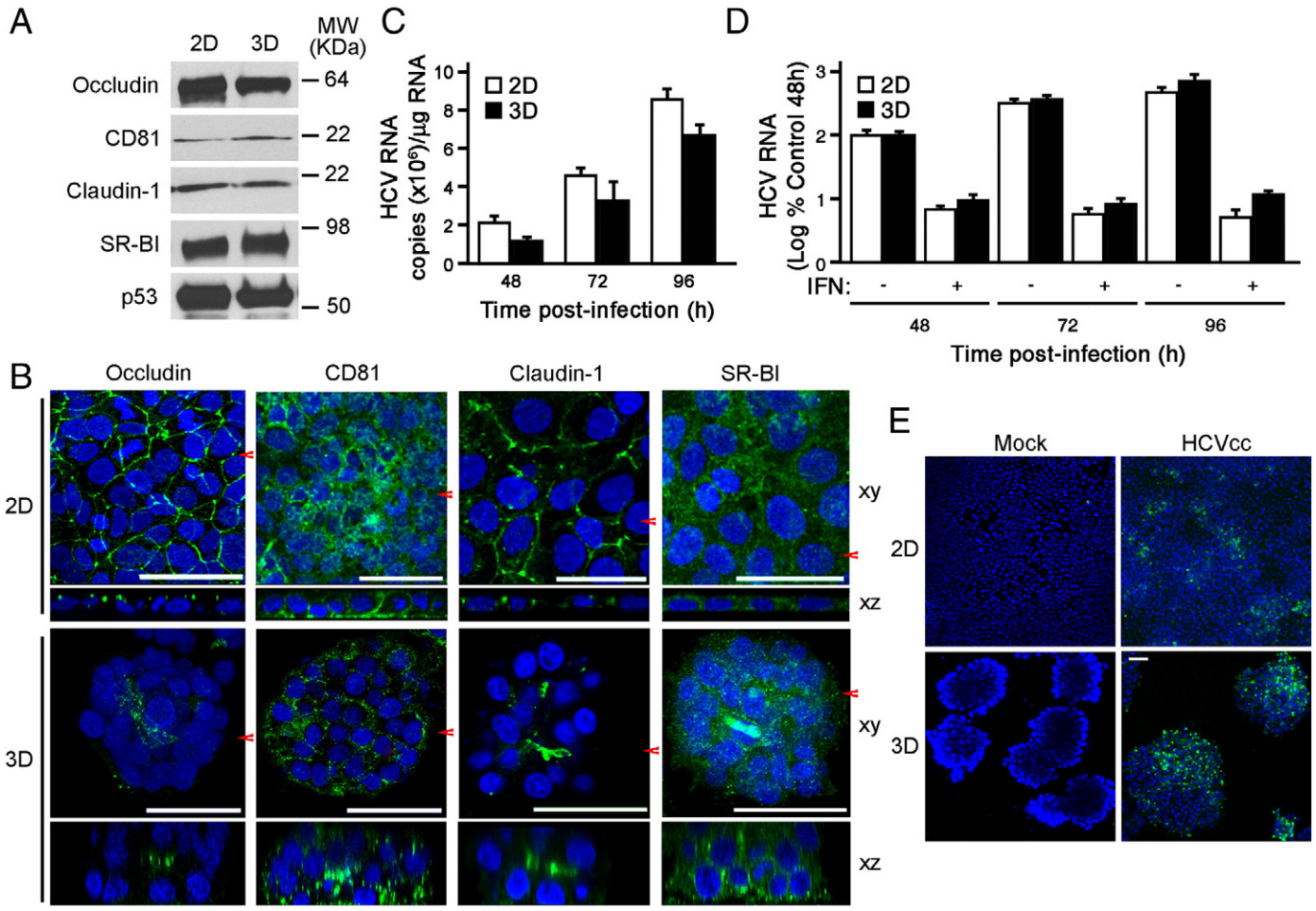

Fig. 3. 3D-cultured Huh-7 cells are susceptible to HCV infection. (A) The expression of HCV (co)receptors (occludin, CD81, claudin-1 and SR-BI) was analyzed by Western blot after 6 days of 2D or 3D culture. p53 was used as loading control. (B) The localization of HCV (co)receptors was analyzed by immunofluorescence and confocal analysis. XY images show the merged projection of confocal stacks. Arrows indicate the planes corresponding to the XZ sections shown. Nuclei were stained with DAPI (blue). Images are representative of three independent experiments. Bar, 50 µm. (C) Cells were grown in 2D or 3D conditions for 6 days and infected overnight with 2D-produced HCVcc. Cells were further cultured for 48, 72 or 96 h post-infection, total RNA was extracted and HCV RNA was quantified by real-time RT-PCR. Data are represented as the mean value ± SD of a triplicate experiment. (D) Cells were cultured and infected as in (C), treated with 350 UI/ml of human IFN-α2b where indicated and HCV RNA was quantified as in (C). Data are represented as the mean value ± SD of a triplicate experiment. (E) Cells were cultured in 2D or 3D conditions for 6 days and infected with HCVcc. A mock infection control was included. Three days after infection, cells were processed for immunostaining using anti-core specific Ab (green). Nuclei were stained with DAPI (blue). Images show the merged projection of confocal stacks. Bar, 50 µm. Results are representative of two separate experiments.

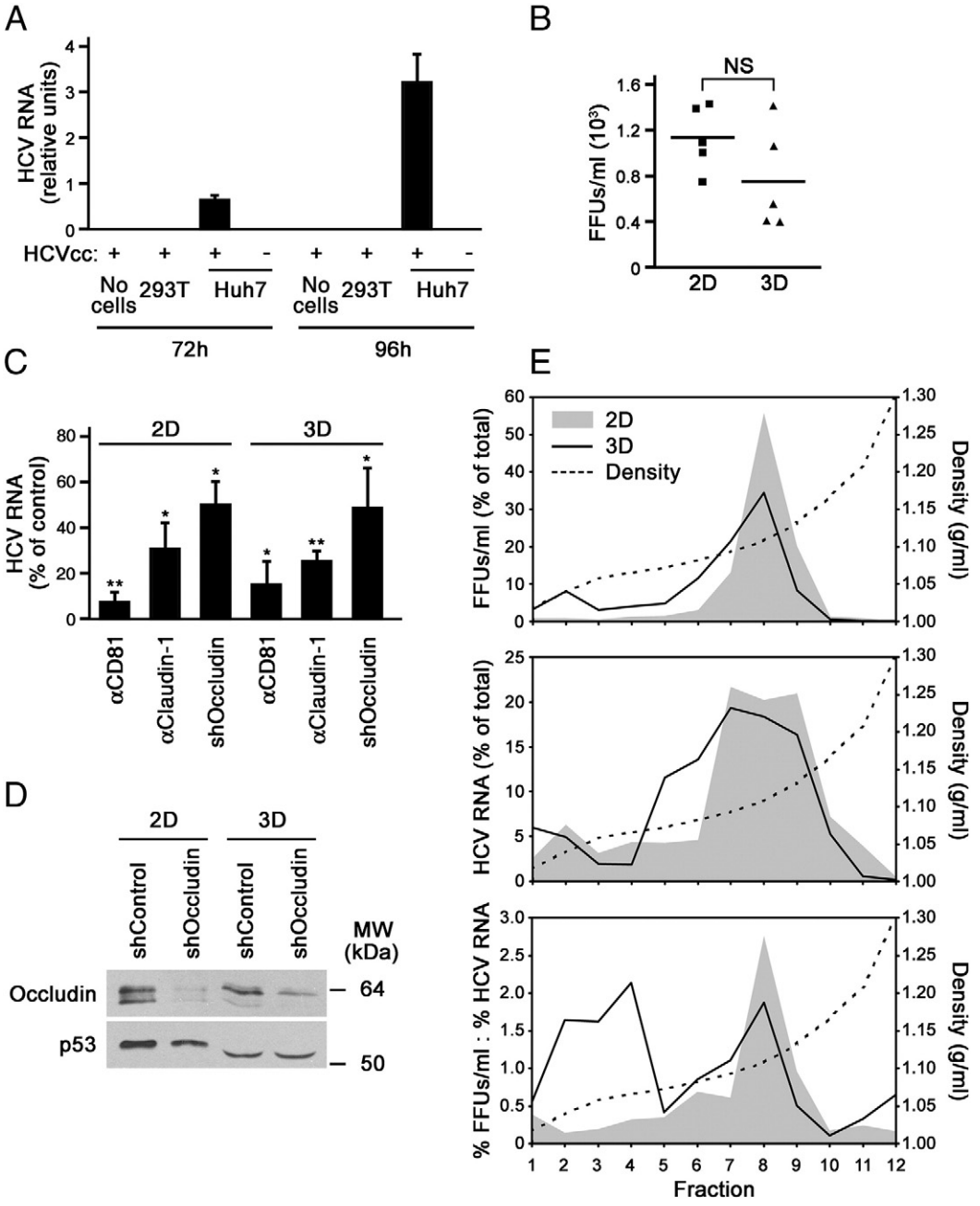

Fig. 4. Viral particle production by 3D cultures and comparison with 2D-generated HCVcc. (A) 3D cultures were performed with no cells and either 293T or Huh-7 cells. After 6 days, cultures were infected overnight with 2D-generated HCVcc, washed and fresh complete medium was added. 72 and 96 h post-infection, culture supernatants were harvested, filtered and used to infect naïve 2D-cultured Huh-7 cells. HCV RNA levels in target cells were determined 72 h later by real-time RT-PCR. Data are represented as the mean value ± SD of a triplicate experiment. (B) Huh-7 cells were cultured in 2D or 3D conditions for 6 days and infected overnight with 2D-produced HCVcc. After washing, cells were cultured for 96 h and supernatants were harvested, filtered and titrated on 2D-cultured Huh-7.5 cells. Data from five independent viral productions are expressed as focus forming units (FFUs)/ml and plotted as black squares (2D) or triangles (3D) including the mean values (horizontal lines). NS, not statistically significant ($P = 0.175$ vs. 2D, Mann–Whitney U test). (C) HCVcc was produced in 2D or 3D conditions as in (B) and used to infect naïve Huh-7 cells that had been cultured in 2D or 3D conditions, respectively, for 6 days. Incubation of cultures with 2 μg/ml anti-CD81 or isotype control, or a 1/100 dilution of anti-claudin-1 or control serum, was performed 1 h prior 2D or 3D-produced HCVcc infection. Retroviral transduction of control and occludin shRNAs was performed twice, 32 and 8 h before target cell seeding. HCV RNA levels were measured by real-time RT-PCR 72 h after infection. Results are presented as the percentage of infection of control antibody, serum or shRNA. Data are represented as the mean value ± SEM of at least three independent experiments performed in triplicate. *, $P<0.05$; **, $P<0.01$ versus control, paired t-test. (D) Occludin knockdown efficiency was evaluated by Western blot at the moment of 2D or 3D-produced HCVcc infection. p53 was used as loading control. (E) Viral supernatants from 2D (gray area) and 3D (solid line) cultures were subjected to ultracentrifugation through 0–40% iodixanol gradients. Fractions were used to measure infectivity (top panel) and HCV RNA levels (middle panel). FFUs, focus forming units. Values for each fraction are expressed as the percentage of the total of the gradient. Density is plotted as a dotted line in all panels. Data are represented as the mean value of at least four independent experiments. The bottom panel represents the ratio between infectivity (top panel) and HCV RNA levels (middle panel).

HCVcc RNA. Furthermore, HCV RNA levels dropped more than ten fold in the presence of IFN-α (Fig. 3D), strongly suggesting that productive infection and active replication was taking place in both 2D and 3D conditions. In order to compare HCV replication in 2D and 3D cultures, HCV replicon-containing cells were cultured in both conditions and viral RNA was measured by real-time RT-PCR. No differences were observed between 2D and 3D cultures (Supplementary Fig. S4). Therefore, these data indicated that 3D-cultured cells could be productively infected by HCVcc and supported viral spread to a similar extent as 2D cultures, and that viral RNA replication was not affected by embedding cells in

Matrigel. To further confirm the susceptibility of spheroids to be infected, we performed immunofluorescence analysis of the viral core protein in mock or HCVcc-infected Huh-7 cells cultured in 2D or 3D conditions (Fig. 3E). After HCVcc challenge, we clearly observed viral protein-positive cells, demonstrating that 3D cultures were permissive for HCVcc infection.

Characterization of HCVcc produced by 3D-cultured cells

We then investigated the possible release of infectious virions from HCVcc-infected spheroids. We found that supernatants derived from HCVcc-infected Huh-7 spheroids were infective, and that those collected 96 h after infection were more infective than when harvested 72 h post-infection (Fig. 4A). Of note, supernatants derived from HCVcc-challenged Matrigel without cells or 3D-cultured 293T cells, which are not susceptible to HCVcc infection (Evans et al., 2007), were not infective (Fig. 4A). These data ruled out the possibility that supernatant infectivity was due to carry-over HCVcc from the inoculum. Additionally, side-by-side experiments with 2D and 3D cultures showed that HCVcc-infected 3D-cultured cells were able to generate infectious supernatants with similar titers (~10^3 FFUs/ml) as standard 2D cultures (Fig. 4B). Next, we wanted to determine whether molecules known to mediate HCV entry in standard 2D conditions are also necessary in a 3D context. As shown in Fig. 4C, anti-claudin-1 serum and anti-CD81 antibody inhibited HCVcc infection in both 2D and 3D cultures to a comparable extent. Similarly, occludin knockdown (Fig. 4D) markedly reduced the susceptibility of 2D and 3D-cultured Huh-7 cells to HCVcc infection. These data strongly suggested that CD81, claudin-1 and occludin participated in HCVcc infection of hepatocyte-like polarized cultures.

Finally, in order to determine the density profile of 2D and 3D-generated HCVcc, culture supernatants were subjected to ultracentrifugation through continuous iodixanol gradients. The infectivity and HCV RNA content of each fraction was evaluated by titration on Huh-7.5 cells and real-time RT-PCR, respectively. Whereas infectivity of both 2D and 3D-produced HCVcc peaked at 1.107 g/ml, fractions below 1.107 g/ml obtained in 3D conditions consistently presented a higher associated infectivity than those derived from 2D cultures (Fig. 4E, top). Interestingly, 3D culture-derived supernatants showed an almost 6-fold increase in the relative infectivity of fractions between 1.017 and 1.058 g/ml compared to 2D conditions (Table 1). Additionally, HCV RNA peaked between 1.094 and 1.132 g/ml in both conditions, but 3D-obtained fractions between 1.072 and 1.082 g/ml contained approximately 3-fold higher viral RNA levels than their 2D counterparts (Fig. 4E, middle). When a ratio between infectivity and HCV RNA was calculated, values obtained from fractions ≥1.072 g/ml were similar in both conditions (Fig. 4E, bottom); however, 3D-derived fractions between 1.04 and 1.066 g/ml presented approximately 7- to 12-fold higher values than 2D-obtained fractions (Fig. 4E, bottom). Collectively, these data suggested that 3D-generated HCVcc shifted towards lower densities, and that specific infectivity between 1.04 and 1.066 g/ml was markedly increased in these conditions.

Table 1
Density range and relative infectivity of grouped fractions from 2D and 3D-produced viral supernatants. Viral supernatants from 2D and 3D cultures were subjected to ultracentrifugation through 0–40% iodixanol gradients. The density and infectivity of each fraction were determined and grouped as indicated. Values for each group are expressed as the percentage of the total of the gradient.

Fractions	Density (g/ml)#	FFUs/ml (% of total)#	
		2D	3D
1–3	1.017 (± 0.001) ≤ d ≤ 1.058 (± 0.002)	2.5 ± 1.1	14.5 ± 5.0*
4–6	1.066 (± 0.002) ≤ d ≤ 1.082 (± 0.002)	6.0 ± 2.7	20.4 ± 7.5
7–9	1.094 (± 0.002) ≤ d ≤ 1.132 (± 0.005)	89.1 ± 3.1	64.2 ± 10.9
10–12	1.166 (± 0.006) ≤ d ≤ 1.302 (± 0.009)	2.3 ± 0.8	0.9 ± 0.3

#, mean ± SEM (n = 5); *, $P<0.05$ vs. 2D, Mann–Whitney *U* test.

Discussion

The ability to modulate hepatocyte polarity and multicellular organization is important for developing in vitro systems designed to reproduce liver functions (Decaens et al., 2008). Extracellular matrix modulates various cellular processes including polarization and cell metabolism, and has been shown to maintain the phenotype of hepatocytes in culture (Castell and Gomez-Lechon, 2009). Herein, we demonstrate that Matrigel-embedded 3D cultures of Huh-7 cells, in contrast to standard 2D conditions, form polarized aggregates that develop TJ-delimited BC-like structures and are susceptible to HCVcc infection, constituting an improved system for the study of HCV and the virus-host interaction. In addition, it emerges as a suitable model to further characterize the contribution of polarity and TJ-associated proteins to HCV infection in a hepatocytic polarization context. Matrigel-embedded 3D aggregates are also able to produce infectious HCVcc particles. Moreover, infection in a 3D-context (i. e., 3D-generated virions employed to infect 3D cultures) is shown to be CD81, claudin-1 and occludin-dependent. These data strongly suggest that CD81, claudin-1 and occludin participate in HCVcc infection of cultures with hepatocytic polarization. These results are in agreement with recent studies in which serum-derived HCV infection of primary human hepatocytes (PHH) was claudin-1 and CD81 dependent (Fofana et al., 2010; Molina et al., 2008). To our knowledge, this is the first demonstration that occludin is implicated in HCV infection of hepatocyte-like polarized cultures.

In plasma, HCV RNA-containing particles exhibit a wide range of density from 1.03 to 1.30 g/ml (Andre et al., 2005). This heterogeneity has been attributed to a varying ratio of virions to non-enveloped cores and their variable association with host lipoproteins and/or immunoglobulins (Andre et al., 2005). Interestingly, in the serum of an immunodeficient, anti-HCV negative patient the majority of viral RNA was found below 1.08 g/ml (Nielsen et al., 2006). Additionally, a similarly narrow density range (<1.063 g/ml) was observed in a chimpanzee with a HCV acute infection prior to the onset of immune responses (Hijikata et al., 1993). In contrast, viral RNA from HCVcc peaks at ~1.15 g/ml (Gastaminza et al., 2006; Lindenbach et al., 2005, 2006; Wakita et al., 2005). Given that the higher density of in vitro-produced HCVcc could not be due to the presence of immunoglobulins complexed with the virions, these data suggest that HCVcc may differ from real HCV in terms of lipoprotein association and/or the percentage of total HCV RNA associated to naked capsids. Therefore, infectivity associated to high density HCVcc might correspond to viral particles that are significantly different from real virions, thus altering the readout of experiments. In this work, we have shown that both infectivity and viral RNA from 3D-generated HCVcc shift towards lower densities than HCVcc produced in 2D conditions. Similar results have been reported with viral particles obtained from either PHH (Podevin et al., 2010) or plasma from animals inoculated with standard HCVcc (Lindenbach et al., 2006). Moreover, we have shown that between 1.04 and 1.066 g/ml (fractions 2–4), despite similar relative levels of HCV RNA were found in both 2D and 3D conditions, the ratio infectivity/viral RNA was 7- to 12-fold higher for 3D-generated virions. This result suggests that infectivity of low density viral particles is higher when they derive from 3D cultures, observation which correlates well with the fact that particle density is inversely correlated to infectivity in vivo (Hijikata et al., 1993). Collectively, these data indicate that the nature of host cells may determine some properties of the progeny virus, and that virions generated in a more physiological context better resemble natural HCV.

The very low density of some natural HCV particles has been attributed to an association of the virus with ApoB and/or ApoE-positive triglyceride-rich lipoproteins (Andre et al., 2002, 2005; Chang et al.,

2007; Diaz et al., 2006) that might take place during viral egress (Gastaminza et al., 2008). Similar properties have also been reported with in vitro produced HCVcc in which virions were found to be secreted in a manner that parallels the formation of very low density lipoproteins (VLDLs) (Chang et al., 2007; Gastaminza et al., 2006, 2008; Meunier et al., 2008). On the other hand, early reports established a link among cell polarization, lipoprotein secretion and virus assembly. In highly polarized Caco-2 cells, lipoprotein secretion was shown to be a vectorial process mainly taking place across the basolateral membrane (Traber et al., 1987), and it could be enhanced by extracellular matrix proteins (Ratcliffe et al., 2009). In addition, assembly of RNA enveloped viruses in MDCK cells was proved to be closely related to cell polarization (Rodriguez-Boulan et al., 1983). Thus, it is reasonable to hypothesize that the lack of hepatocytic polarization of hepatoma-derived 2D-cultured cells could be responsible for a defective secretion of lipoproteins, which could in turn affect the correct assembly and egress of viral particles. In fact, it has been demonstrated that, in contrast to Huh-7 and Huh-7.5 cells, the polarized cell lines HepG2 and Caco-2 can secrete HCV glycoproteins in association with ApoB (Icard et al., 2009). Furthermore, Huh-7-derived cells have proved to be unable to secrete authentic, ApoB-containing VLDLs (Podevin et al., 2010). Interestingly, the different biophysical properties observed between 2D and 3D-generated virions were not related to major changes in differentiation-specific gene expression, but were most likely due to the modulation of the polarization state of virus-producing cells. This finding points to the existence of a direct link between HCV assembly and/or egress and cellular polarization regardless of the differentiation state. In summary, these observations suggest that in vitro-obtained viral particles from non-polarized cell lines may differ from both natural HCV and virions obtained from polarized cells in terms of lipoprotein composition or configuration within the lipoviroparticle, hypothesis which is currently being studied in our laboratory. This might explain why, in contrast to 2D-produced HCV pseudotyped particles, HCV-like particles and HCVcc, infection with serum-derived HCV is an LDL receptor-dependent process (Bartosch et al., 2003; Hsu et al., 2003; Molina et al., 2007; Triyatni et al., 2002; von Hahn et al., 2006).

Conclusions

It is largely assumed that PHH-derived systems are the best models to mimic natural HCV infection. However, working with PHH presents several limitations apart from ethical concerns and logistics requirements, including interindividual variability and differences in the quality of the available tissue that make it difficult to standardize both the isolation procedure and the obtained results (Gondeau et al., 2009). Studying HCV life cycle in Huh-7-derived 3D cultures presents the advantages of working with a cell line (homogeneity, unlimited availability, robust replication and virion production, easy genetic manipulation and the possibility of performing long term experiments) whilst maintaining hepatocytic polarity. Additionally, at least some characteristics of 3D-produced HCVcc are similar to those of natural HCV, thus providing a more physiologically relevant context than standard 2D cultures. Therefore, we propose Matrigel-embedded 3D Huh-7 cultures as a practical system that could be used as a first screen before validating data with PHH. We expect that this novel, easy-made, high throughput-adaptable and reliable model will provide a valuable tool to understand the mechanisms governing hepatocyte HCV infection.

Materials and methods

Cell culture, generation of HCV replicon-containing clones and HCVcc infection

293T cells and the human hepatocyte-derived cell line Huh-7 were grown at 37 °C with a 5% CO2 atmosphere in Dulbecco's modified Eagle's medium (DMEM), supplemented with 10% fetal calf serum, 2 mM L-glutamine, 50 μg/ml gentamycin, 100 U/ml penicillin and 100 μg/ml streptomycin. For 3D Matrigel-embedded cultures, 50 μl of complete medium containing 5×10^3 cells was added to 50 μl of Growth factor-reduced Matrigel with a protein concentration ranging from 7 to 7.5 μg/μl (BD Biosciences), gently mixed and deposited into either a 8-well chambered coverglass (Nalge Nunc International) or a 48-well plate (Corning Incorporated) depending on the experiment and incubated at 37 °C for 30 min. For some experiments, 3D cultures were scaled to 24-well plates using 100 μl of complete medium containing 10^4 cells and 100 μl of Matrigel (see below). Cells were then covered with complete medium and grown at 37 °C under 5% CO2 for 6 or 9 days, changing medium every 2 days. Huh-7 cells expressing full-length or subgenomic genotype 1b (Con1, EMBL database accession number AJ238799) HCV replicons were established as previously described (Benedicto et al., 2008). JFH1 HCVcc was produced as previously described (Benedicto et al., 2008) and expanded in culture for several passages. For HCVcc infection assays, 5×10^3 cells were grown on 2D (24-well plates) or 3D (48-well plates) cultures for 6 days. Where indicated, anti-CD81 antibody (clone JS-81, BD Biosciences), MOPC-21 mouse isotype control (Sigma), polyclonal anti-claudin-1 or preimmune sera (Krieger et al., 2010) were added 1 h before infection, and cultures were infected with 10^3 FFUs overnight. Medium was changed and 350 UI/ml of human IFN-α2b (PEG-Intron, Schering-Plough Corp.) was added where indicated and replenished every 24 h. At different times post-infection cells were processed for real-time RT-PCR or immunofluorescence (see below).

Immunofluorescence analysis and confocal microscopy

Cells were grown in chambered coverglasses with or without Matrigel for 6 or 9 days. Cells were fixed with 2% paraformaldehyde for 20 min at room temperature and permeabilized with 0.5% TritonX-100 in PBS for 10 min at room temperature. Cells were rinsed three times with 100 mM glycine in PBS for 15 min and blocked with TNB [0.1 M Tris–HCl, 0.15 M NaCl, 0.5% blocking reagent (Boehringer Mannheim GmbH)] plus 10% goat serum from Sigma for 2 h at 37 °C. Cells were incubated with the indicated antibodies diluted in TNB overnight at room temperature and after washing with 0.1% NP-40 in PBS, cells were incubated with Alexa 488, Alexa 647 or rhodamine X-conjugated goat anti-mouse or anti-rabbit antibodies (Molecular Probes, Inc.) for 2 h at 37 °C and counterstained with DAPI (Pierce). For multiple stainings, samples were incubated sequentially with the indicated primary and secondary antibodies. The preparations were analyzed with a Leica TCS-SP5 (Leica Microsystems) confocal microscope. Antibodies used were: monoclonal anti-Na^+, K^+-ATPase (Abcam), anti-GM130 (BD Bioscencies), anti-MRP2 (M2 III-6; Alexis Laboratories), anti-CD81 (clone 1.3.3.22, Santa Cruz Biotechnology), anti-occludin (Zymed), polyclonal anti-radixin (Cell Signaling Technology), anti-ZO-1, anti-occludin, anti-claudin-1 (Zymed), anti-SR-BI (Novus Biologicals) and the monoclonal antibody against HCV core (clone C7-50, Affinity BioReagents) protein.

Western blots

5×10^3 cells were grown on 48-well plates for 3D Matrigel cultures or 24-well plates for 2D conventional cultures for 6 to 9 days. Cells were lysed on the plate with 100 μl of Laemmli buffer and boiled for 5 min. Western blots were carried out as previously described (Benedicto et al., 2008) with the following antibodies: polyclonal anti-occludin, anti-claudin-1 and anti-SR-BI and monoclonal anti-MRP2 (see above), anti-CD81 (clone 5A6) and anti-p53 (Santa Cruz Biotechnology).

Characterization of hepatocyte-like polarity

Functional BC, those that exhibited an accumulation of 5-chloromethylfluorescein di-acetate (CMFDA) or cholylglycylamido fluorescein (CGamF), were determined by confocal analysis of fluorescent compounds (Bogman et al., 2003; Bravo et al., 1998; Lindenmaier et al., 2005). The nonfluorescent lipophilic CMFDA (Molecular Probes) passively penetrates the plasma membrane. Inside the cells, cytosolic esterases cleave off its acetate residues, thereby releasing the fluorescent and membrane-impermeable product 5-chloromethylfluorescein (CMF), which can react (e.g., with glutathione) to form fluorescent conjugates. This methylfluorescein-glutathione complex is then actively secreted by MRP2 (Bogman et al., 2003). The conjugated bile salt CGamF was synthesized by binding FITC to glycocholate at the carboxyl group following a previously described method (Sherman and Fisher, 1986). This fluorescent bile salt derivative has been used to determine hepatocyte polarity-associated vectorial transport towards BC-like structures into which CGamF is secreted (Cantz et al., 2000). Cells were grown into chambered coverglasses with or without Matrigel for 6 days and incubated with 5 μM of either CMFDA or CGamF in culture medium for 20 min at 37 °C. Cells were rinsed four times with fresh medium in the presence (5 mM) or absence of the MRP2 inhibitor Probenecid (Sigma) where indicated and the accumulation of fluorescent products was analyzed with a confocal microscope.

RT-PCR

RNA extraction, reverse transcription and quantitative PCR were performed as previously described (Benedicto et al., 2008). Specific primers used were: HCV, H3 (Benedicto et al., 2008) and MRP2 (Briz et al., 2007) as previously described; HNF4α, 5′-CGGAAGAACCACATGTACTC-3′ and 5′-TGCTGTCCTCATAGCTTGAC-3′; α1AT, 5′-TCAAGGAGCTTGACAGAGAC-3′ and 5′-GACAGCTTCTTACAGTGCTG-3′; TTR, 5′-GCTGGACTGGTATTTGTGTC-3′ and 5′-ACTCACTGGTTTTCCCAGAG-3′; albumin, 5′-TGTGTTGCTGATGAGTCAGC-3′ and 5′-ACATCAACCTCTGGTCTCAC-3′; CYP3A5, 5′-GGAGAGCACTAAGAAGTTCC-3′ and 5′-TGTCGTTGAGGCGACTTTTC-3′; UGT1A1, 5′-ACAGAACTTTCTGTGCGACG-3′ and 5′-CCACAATTCCATGTTCTCCAG-3′. Histone H3 mRNA levels were used for sample normalization.

Short hairpin RNA (shRNA) retroviral transfer

Generation of control and occludin shRNA retroviral vectors, production of retroviral particles and infection was performed as previously described (Benedicto et al., 2009). 5×10^3 transduced cells were reseeded in 2D (24-well plates) or 3D (48-well plates) cultures 8 h after the last transduction. Cells were grown for 6 days and either infected with HCVcc or lysed to check knockdown efficiency by Western blot (see above).

Iodixanol gradient ultracentrifugation of 2D and 3D-generated HCVcc

10^4 cells were seeded in 2D (12-well plates) and 3D (24-well plates) conditions. After 6 days, cells were HCVcc infected overnight, washed and 1 ml of complete medium per well was added. 96 h post-infection the supernatants were harvested, filtered through 0.45-μm pore-sized membranes and concentrated 5-fold in a 100,000 molecular weight cut-off Spin-X UF 6 Concentrator (Corning Incorporated) at 4 °C. Continuous 0–40% iodixanol gradients were prepared using Optiprep (Axis-Shield). 5.5 ml of 40% iodixanol in 83 mM sucrose, 1 mM EDTA and 10 mM Tris–HCl pH 7.4 were layered with 5.5 ml of homogenization media (250 mM sucrose, 1 mM EDTA and 10 mM Tris–HCl pH 7.4) and the gradients were formed with a Gradient Master (BioComp Instruments, Inc.). 1 ml of the concentrated viral supernatant was loaded on top of the gradient and tubes were subjected to ultracentrifugation in a SW41 rotor (Beckman Coulter) at 31,000 rpm and 4 °C for 16 h. 1 ml fractions were collected from the top and titration was performed by infection of Huh-7.5 cells with serially diluted fractions and staining with anti-core antibody. Viral RNA levels were measured by extracting RNA from 100 μl of each fraction with 900 μl of TRI Reagent (Ambion Inc.), using 20 μg of glycogen (Roche Diagnostics GmbH) as a carrier for RNA precipitation, and performing real-time RT-PCR (see above). Density of fractions was calculated using a refractometer (EUROMEX microscopen BV).

Supplementary materials related to this article can be found online at doi:10.1016/j.virol.2011.12.021

Acknowledgments

This work was supported in part by grants : 1) CIBERehd [ISCIII] to R. Moreno-Otero, M. López-Cabrera and P. L. Majano; 2) SAF2007-61201 [Ministerio de Educación y Ciencia] to M. López-Cabrera; 3) Agence Nationale pour la Recherche contre le SIDA et les Hépatites Virales (ANRS) to F. L. Cosset; 4) European Research Council (ERC-2008-AdG-233130-HEPCENT) to F. L. Cosset; 5) SAF2007-60677 [Ministerio de Educación y Ciencia]; 6) PI10/00101 [ISCIII] to P. L. Majano. and 7) Fundación Mutua Madrileña to P.L. Majano I. Benedicto was financially supported by CIBERehd and F. Molina-Jiménez by ISCIII and FIB Hospital Universitario de la Princesa. V. L. Dao Thi is supported by a pre-doctoral fellowship from Région Rhône-Alpes (ClusterX). The authors express their gratitude to R. Bartenschlager and T. Wakita for providing us with critical reagents, A. Aguilera and J. Loureiro for statistical analysis and P. Gastaminza for helpful discussion and comments on the manuscript.

References

Aijaz, S., Balda, M.S., Matter, K., 2006. Tight junctions: molecular architecture and function. Int. Rev. Cytol. 248, 261–298.
Andre, P., Komurian-Pradel, F., Deforges, S., Perret, M., Berland, J.L., Sodoyer, M., Pol, S., Brechot, C., Paranhos-Baccala, G., Lotteau, V., 2002. Characterization of low- and very-low-density hepatitis C virus RNA-containing particles. J. Virol. 76, 6919–6928.
Andre, P., Perlemuter, G., Budkowska, A., Brechot, C., Lotteau, V., 2005. Hepatitis C virus particles and lipoprotein metabolism. Semin. Liver Dis. 25, 93–104.
Bartosch, B., Dubuisson, J., Cosset, F.L., 2003. Infectious hepatitis C virus pseudo-particles containing functional E1–E2 envelope protein complexes. J. Exp. Med. 197, 633–642.
Benedicto, I., Molina-Jimenez, F., Barreiro, O., Maldonado-Rodriguez, A., Prieto, J., Moreno-Otero, R., Aldabe, R., Lopez-Cabrera, M., Majano, P.L., 2008. Hepatitis C virus envelope components alter localization of hepatocyte tight junction-associated proteins and promote occludin retention in the endoplasmic reticulum. Hepatology 48, 1044–1053.
Benedicto, I., Molina-Jimenez, F., Bartosch, B., Cosset, F.L., Lavillette, D., Prieto, J., Moreno-Otero, R., Valenzuela-Fernandez, A., Aldabe, R., & other authors, 2009. The tight junction-associated protein occludin is required for a postbinding step in hepatitis C virus entry and infection. J. Virol. 83, 8012–8020.
Bogman, K., Erne-Brand, F., Alsenz, J., Drewe, J., 2003. The role of surfactants in the reversal of active transport mediated by multidrug resistance proteins. J. Pharm. Sci. 92, 1250–1261.
Bravo, P., Bender, V., Cassio, D., 1998. Efficient in vitro vectorial transport of a fluorescent conjugated bile acid analogue by polarized hepatic hybrid WIF-B and WIF-B9 cells. Hepatology 27, 576–583.
Briz, O., Cassio, D., Blazquez, A.G., Grosse, B., Serrano, M.A., Marin, J.J., 2007. Characterization of WIF-B9/R cells as an in vitro model with hepatocyte-like polarity and enhanced expression of canalicular ABC transporters involved in phase III of hepatic detoxification. Toxicology 232, 24–36.
Cantz, T., Nies, A.T., Brom, M., Hofmann, A.F., Keppler, D., 2000. MRP2, a human conjugate export pump, is present and transports fluo 3 into apical vacuoles of Hep G2 cells. Am. J. Physiol. Gastrointest. Liver Physiol. 278, G522–G531.
Castell, J.V., Gomez-Lechon, M.J., 2009. Liver cell culture techniques. Methods Mol. Biol. 481, 35–46.
Chang, K.S., Jiang, J., Cai, Z., Luo, G., 2007. Human apolipoprotein e is required for infectivity and production of hepatitis C virus in cell culture. J. Virol. 81, 13783–13793.
Decaens, C., Durand, M., Grosse, B., Cassio, D., 2008. Which in vitro models could be best used to study hepatocyte polarity? Biol. Cell 100, 387–398.
Diaz, O., Delers, F., Maynard, M., Demignot, S., Zoulim, F., Chambaz, J., Trepo, C., Lotteau, V., Andre, P., 2006. Preferential association of hepatitis C virus with apolipoprotein B48-containing lipoproteins. J. Gen. Virol. 87, 2983–2991.
Easter, D.W., Wade, J.B., Boyer, J.L., 1983. Structural integrity of hepatocyte tight junctions. J. Cell Biol. 96, 745–749.

Evans, M.J., von Hahn, T., Tscherne, D.M., Syder, A.J., Panis, M., Wolk, B., Hatziioannou, T., McKeating, J.A., Bieniasz, P.D., Rice, C.M., 2007. Claudin-1 is a hepatitis C virus co-receptor required for a late step in entry. Nature 446, 801–805.
Feld, J.J., Hoofnagle, J.H., 2005. Mechanism of action of interferon and ribavirin in treatment of hepatitis C. Nature 436, 967–972.
Fofana, I., Krieger, S.E., Grunert, F., Glauben, S., Xiao, F., Fafi-Kremer, S., Soulier, E., Royer, C., Thumann, C., & other authors, 2010. Monoclonal anti-claudin 1 antibodies prevent hepatitis C virus infection of primary human hepatocytes. Gastroenterology 139, 953–964.
Gastaminza, P., Kapadia, S.B., Chisari, F.V., 2006. Differential biophysical properties of infectious intracellular and secreted hepatitis C virus particles. J. Virol. 80, 11074–11081.
Gastaminza, P., Cheng, G., Wieland, S., Zhong, J., Liao, W., Chisari, F.V., 2008. Cellular determinants of hepatitis C virus assembly, maturation, degradation, and secretion. J. Virol. 82, 2120–2129.
Gondeau, C., Pichard-Garcia, L., Maurel, P., 2009. Cellular models for the screening and development of anti-hepatitis C virus agents. Pharmacol. Ther. 124, 1–22.
Harris, H.J., Davis, C., Mullins, J.G., Hu, K., Goodall, M., Farquhar, M.J., Mee, C.J., McCaffrey, K., Young, S., & other authors, 2010. Claudin association with CD81 defines hepatitis C virus entry. J. Biol. Chem. 285, 21092–21102.
Hijikata, M., Shimizu, Y.K., Kato, H., Iwamoto, A., Shih, J.W., Alter, H.J., Purcell, R.H., Yoshikura, H., 1993. Equilibrium centrifugation studies of hepatitis C virus: evidence for circulating immune complexes. J. Virol. 67, 1953–1958.
Hofmann, W.P., Zeuzem, S., 2011. A new standard of care for the treatment of chronic HCV infection. Nat. Rev. Gastroenterol. Hepatol. 8, 257–264.
Hsu, M., Zhang, J., Flint, M., Logvinoff, C., Cheng-Mayer, C., Rice, C.M., McKeating, J.A., 2003. Hepatitis C virus glycoproteins mediate pH-dependent cell entry of pseudotyped retroviral particles. Proc. Natl. Acad. Sci. U. S. A. 100, 7271–7276.
Icard, V., Diaz, O., Scholtes, C., Perrin-Cocon, L., Ramiere, C., Bartenschlager, R., Penin, F., Lotteau, V., Andre, P., 2009. Secretion of hepatitis C virus envelope glycoproteins depends on assembly of apolipoprotein B positive lipoproteins. PLoS One 4, e4233.
Kleinman, H.K., Martin, G.R., 2005. Matrigel: basement membrane matrix with biological activity. Semin. Cancer Biol. 15, 378–386.
Krieger, S.E., Zeisel, M.B., Davis, C., Thumann, C., Harris, H.J., Schnober, E.K., Mee, C., Soulier, E., Royer, C., & other authors, 2010. Inhibition of hepatitis C virus infection by anti-claudin-1 antibodies is mediated by neutralization of E2-CD81-claudin-1 associations. Hepatology 51, 1144–1157.
Lindenbach, B.D., Rice, C.M., 2005. Unravelling hepatitis C virus replication from genome to function. Nature 436, 933–938.
Lindenbach, B.D., Evans, M.J., Syder, A.J., Wolk, B., Tellinghuisen, T.L., Liu, C.C., Maruyama, T., Hynes, R.O., Burton, D.R., & other authors, 2005. Complete replication of hepatitis C virus in cell culture. Science 309, 623–626.
Lindenbach, B.D., Meuleman, P., Ploss, A., Vanwolleghem, T., Syder, A.J., McKeating, J.A., Lanford, R.E., Feinstone, S.M., Major, M.E., & other authors, 2006. Cell culture-grown hepatitis C virus is infectious in vivo and can be recultured in vitro. Proc. Natl. Acad. Sci. U. S. A. 103, 3805–3809.
Lindenmaier, H., Becker, M., Haefeli, W.E., Weiss, J., 2005. Interaction of progestins with the human multidrug resistance-associated protein 2 (MRP2). Drug Metab. Dispos. 33, 1576–1579.
Mee, C.J., Harris, H.J., Farquhar, M.J., Wilson, G., Reynolds, G., Davis, C., van IJzendoorn, S.C., Balfe, P., McKeating, J.A., 2009. Polarization restricts hepatitis C virus entry into HepG2 hepatoma cells. J. Virol. 83, 6211–6221.
Meunier, J.C., Russell, R.S., Engle, R.E., Faulk, K.N., Purcell, R.H., Emerson, S.U., 2008. Apolipoprotein c1 association with hepatitis C virus. J. Virol. 82, 9647–9656.
Molina, S., Castet, V., Fournier-Wirth, C., Pichard-Garcia, L., Avner, R., Harats, D., Roitelman, J., Barbaras, R., Graber, P., & other authors, 2007. The low-density lipoprotein receptor plays a role in the infection of primary human hepatocytes by hepatitis C virus. J. Hepatol. 46, 411–419.
Molina, S., Castet, V., Pichard-Garcia, L., Wychowski, C., Meurs, E., Pascussi, J.M., Sureau, C., Fabre, J.M., Sacunha, A., & other authors, 2008. Serum-derived hepatitis C virus infection of primary human hepatocytes is tetraspanin CD81 dependent. J. Virol. 82, 569–574.
Narbus, C.M., Israelow, B., Sourisseau, M., Michta, M.L., Hopcraft, S.E., Zeiner, G.M., Evans, M.J., 2011. HepG2 cells expressing microRNA miR-122 support the entire hepatitis C virus life cycle. J. Virol. 85, 12087–12092.
Nielsen, S.U., Bassendine, M.F., Burt, A.D., Martin, C., Pumeechockchai, W., Toms, G.L., 2006. Association between hepatitis C virus and very-low-density lipoprotein (VLDL)/LDL analyzed in iodixanol density gradients. J. Virol. 80, 2418–2428.
Perrault, M., Pecheur, E.I., 2009. The hepatitis C virus and its hepatic environment: a toxic but finely tuned partnership. Biochem. J. 423, 303–314.
Podevin, P., Carpentier, A., Pene, V., Aoudjehane, L., Carriere, M., Zaidi, S., Hernandez, C., Calle, V., Meritet, J.F., & other authors, 2010. Production of infectious hepatitis C virus in primary cultures of human adult hepatocytes. Gastroenterology 139, 1355–1364.
Poynard, T., Yuen, M.F., Ratziu, V., Lai, C.L., 2003. Viral hepatitis C. Lancet 362, 2095–2100.
Ratcliffe, D.R., Iqbal, J., Hussain, M.M., Cramer, E.B., 2009. Fibrillar collagen type I stimulation of apolipoprotein B secretion in Caco-2 cells is mediated by beta1 integrin. Biochim. Biophys. Acta 1791, 1144–1154.
Rodriguez-Boulan, E., Paskiet, K.T., Sabatini, D.D., 1983. Assembly of enveloped viruses in Madin–Darby canine kidney cells: polarized budding from single attached cells and from clusters of cells in suspension. J. Cell Biol. 96, 866–874.
Sainz Jr., B., TenCate, V., Uprichard, S.L., 2009. Three-dimensional Huh7 cell culture system for the study of Hepatitis C virus infection. Virol. J. 6, 103.
Sherman, I.A., Fisher, M.M., 1986. Hepatic transport of fluorescent molecules: in vivo studies using intravital TV microscopy. Hepatology 6, 444–449.
Traber, M.G., Kayden, H.J., Rindler, M.J., 1987. Polarized secretion of newly synthesized lipoproteins by the Caco-2 human intestinal cell line. J. Lipid Res. 28, 1350–1363.
Triyatni, M., Saunier, B., Maruvada, P., Davis, A.R., Ulianich, L., Heller, T., Patel, A., Kohn, L.D., Liang, T.J., 2002. Interaction of hepatitis C virus-like particles and cells: a model system for studying viral binding and entry. J. Virol. 76, 9335–9344.
von Hahn, T., Lindenbach, B.D., Boullier, A., Quehenberger, O., Paulson, M., Rice, C.M., McKeating, J.A., 2006. Oxidized low-density lipoprotein inhibits hepatitis C virus cell entry in human hepatoma cells. Hepatology 43, 932–942.
Wakita, T., Pietschmann, T., Kato, T., Date, T., Miyamoto, M., Zhao, Z., Murthy, K., Habermann, A., Krausslich, H.G., & other authors, 2005. Production of infectious hepatitis C virus in tissue culture from a cloned viral genome. Nat. Med. 11, 791–796.
Wang, W., Soroka, C.J., Mennone, A., Rahner, C., Harry, K., Pypaert, M., Boyer, J.L., 2006. Radixin is required to maintain apical canalicular membrane structure and function in rat hepatocytes. Gastroenterology 131, 878–884.
Zeisel, M.B., Fofana, I., Fafi-Kremer, S., Baumert, T.F., 2011. Hepatitis C virus entry into hepatocytes: molecular mechanisms and targets for antiviral therapies. J. Hepatol. 54, 566–576.